

Nanoscale

Accepted Manuscript



This is an *Accepted Manuscript*, which has been through the Royal Society of Chemistry peer review process and has been accepted for publication.

Accepted Manuscripts are published online shortly after acceptance, before technical editing, formatting and proof reading. Using this free service, authors can make their results available to the community, in citable form, before we publish the edited article. We will replace this *Accepted Manuscript* with the edited and formatted *Advance Article* as soon as it is available.

You can find more information about *Accepted Manuscripts* in the [Information for Authors](#).

Please note that technical editing may introduce minor changes to the text and/or graphics, which may alter content. The journal's standard [Terms & Conditions](#) and the [Ethical guidelines](#) still apply. In no event shall the Royal Society of Chemistry be held responsible for any errors or omissions in this *Accepted Manuscript* or any consequences arising from the use of any information it contains.

ARTICLE

Improved Light Absorption and Charge Transport for Perovskite Solar Cells with Rough Interfaces by Sequential Deposition[†]

Cite this: DOI: 10.1039/x0xx00000x

Lingling Zheng,^a Yingzhuang Ma,^a Saisai Chu,^a Shufeng Wang,^{a,b} Bo Qu,^{a,b} Lixin Xiao,^{a,b*} Zhijian Chen,^{a,b*} Qihuang Gong,^a Zhaoxin Wu,^c and Xun Hou^c

Received 00th January 2012,

Accepted 00th January 2012

DOI: 10.1039/x0xx00000x

www.rsc.org/

Recently, highly efficient solar cells based on organic-inorganic perovskites have been intensively reported on developing fabricating methods and device structures. Additional power conversion efficiency should be gained without increasing the thickness and the complexity of the devices to accord with practical applications. In this paper, a rough interface between perovskite and HTM was fabricated in perovskite solar cells to enhance the light scattering effect and improve the charge transport. The parameters related to the morphology have been systematically investigated by sequential deposition. Simultaneous enhancements of short-circuit current and power conversion efficiency were observed in both $\text{CH}_3\text{NH}_3\text{PbI}_3$ and $\text{CH}_3\text{NH}_3\text{PbI}_{3-x}\text{Cl}_x$ devices containing the rough interface, with power conversion efficiencies of 10.2% and 10.8%, respectively. Our finding provides an efficient and universal way to control the morphology and further optimize perovskite solar cells for devices by sequential deposition with various structures.

Introduction

Hybrid organic-inorganic perovskites, with the form of AMX_3 ($\text{A} = \text{CH}_3\text{NH}_3^+$; $\text{M} = \text{Pb}^{2+}$, or Sn^{2+} ; and $\text{X} = \text{Cl}^-$, Br^- , or I^-), have attracted significant research interest in the field of solar cells. With intense absorptivity from visible to near-infrared region, $\text{CH}_3\text{NH}_3\text{PbI}_3$ and $\text{CH}_3\text{NH}_3\text{PbBr}_3$ were firstly adopted in liquid dye-sensitized solar cells (DSSCs) as the dye-absorbing layer initiated by Miyasaka et al.¹ By using the organic hole transport material (HTM) of 2,2',7,7'-tetrakis(*N,N*-di-*p*-methoxyphenylamine)-9,9'-spirobifluorene (spiro-MeOTAD) to avoid the dissolution of perovskite, much higher power conversion efficiencies (PCEs) have been achieved in solid-state dye-sensitized solar cells.^{2,3} Recently, a mass of researches on optimizing materials, methods and device structures promoted rapid development of PCEs of perovskite solar cells.^{4,23} With a new method of sequential deposition, PCE of 15% was achieved,⁴ and reached 15.7% by using a thin film of ZnO nanoparticles to replace TiO_2 as the electron-transport layer.⁵ The PCEs of solar cells based on perovskite are expected to push toward 20% and then beyond that of crystalline silicon (25%) through better control over all of the processing parameters.⁶

Even though the perovskite based solar cells showed effective light absorption already, additional short-circuit current (J_{sc}) and efficiency can be gained by enhancing the light

absorption, especially in the long-wavelength region. H. J. Snaith et al have employed metal nanoparticles to reduced exciton binding energy, so that the J_{sc} improved without enhancement of light absorption.⁷ M. Grätzel et al used Y^{3+} -substituted mesoporous TiO_2 to affect the crystal growth and improve the perovskite absorber loading, resulting in the higher J_{sc} and IPCE.⁸ However, these methods can only be appropriate for the devices with mesoporous structure, and the usage of Yttrium is disadvantageous for practical applications.

It is well known that highly roughened interface would strengthen internal light scattering, and the larger crystallites and interface area also benefit to the charge transport.^{5,24-26} In this paper, we adjusted the planar perovskite/HTM interface into a rough interface intending to improve the light harvesting and charge transport (Figure 1). It was found that reaction temperature and pre-wetting time were have a great impact on the morphology of the perovskite film by sequential deposition. Under the condition of higher reaction temperature and shorter pre-wetting time, a roughly continuous surface of densely arranged perovskite crystallites with larger size was formed. Simultaneous increases of J_{sc} and PCE were achieved for both $\text{CH}_3\text{NH}_3\text{PbI}_3$ and $\text{CH}_3\text{NH}_3\text{PbI}_{3-x}\text{Cl}_x$ ($x \approx 0.5$) based solar cells, with the PCEs of 10.2% and 10.8%, respectively.

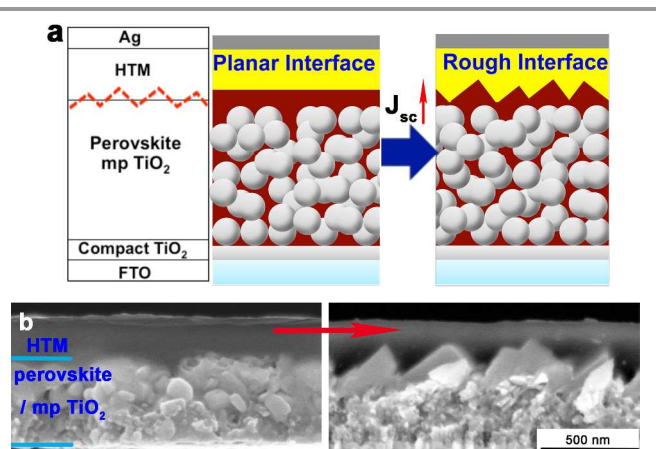


Figure 1. a) Structure diagram of the perovskite solar cell with a perovskite/HTM interface differed from planar to rough b) The cross-sectional SEM images of devices with a perovskite/HTM interface differed from planar to rough.

Results and discussion

In sequential deposition method, the reaction between PbI_2 and $\text{CH}_3\text{NH}_3\text{I}$ and the crystallization of perovskite happen simultaneously. So, different from the light scattering caused by nanostructures on grid electrode,^{27,28} the morphology of perovskite films can be controlled conveniently by changing the reaction and crystallization conditions. Considering the kinetics of crystal growth, both crystallization temperature and the pre-wetting step have a great impact on the crystal size and surface roughness of the resultant film.²⁹ Therefore, both these two ways were adjusted accurately to make the expected rough interface.

1. Reaction temperature control

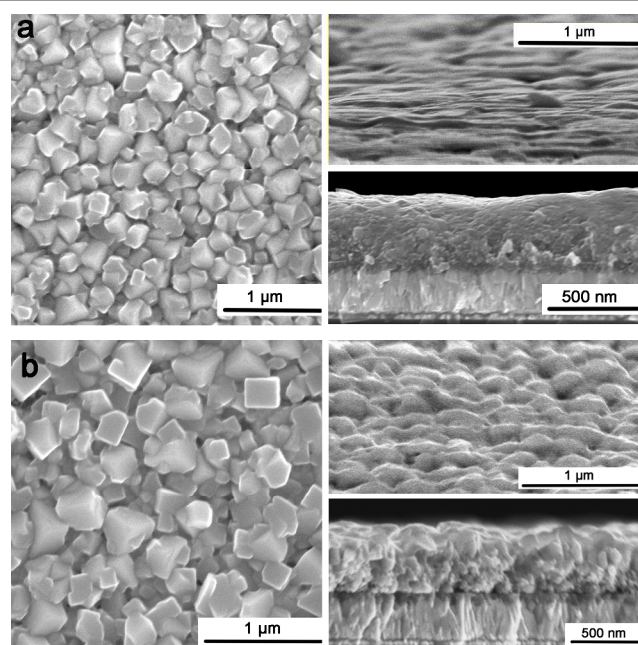


Figure 2. Top-view, side-view, and cross-sectional SEM images of the perovskite layer on top of the mesoporous TiO_2 for a) Film A and b) Film B.

Crystal size can be controlled by the reaction temperature. It was found that at a higher temperature, the crystals were inclined to grow into larger size from the solution due to the faster rate of grain boundaries' migration.²⁹ In order to fabricate perovskite films with different surface roughness, we drenched the prepared $\text{PbI}_2/\text{TiO}_2$ films into $\text{CH}_3\text{NH}_3\text{I}$ solution kept at 25 °C (Film A) and 50 °C (Film B), respectively. The scanning electron microscope (SEM) images from different views of Film A and B are shown in Figure 2.

The SEM images showed that the perovskite crystallites not only filled the mesoporous TiO_2 but also covered it as a continuous layer. With the increase of the reaction temperature, perovskite crystallites with an in-plane grain size of 200 nm in Film A (Figure 2a) enlarged to 350 nm in Film B formed at 50 °C (Figure 2b), leading to a much rougher surface. Tapping-mode atomic force microscopy (AFM) was also employed to obtain more details of the surface morphology. From the 3D topographic images (Figure S3a†), a much rougher surface of Film B was clearly observed and the calculated root mean square (rms) roughness of Film B reached 78.2 nm, much greater than 44.5 nm of Film A by analyzing the height images (Figure S3c†).

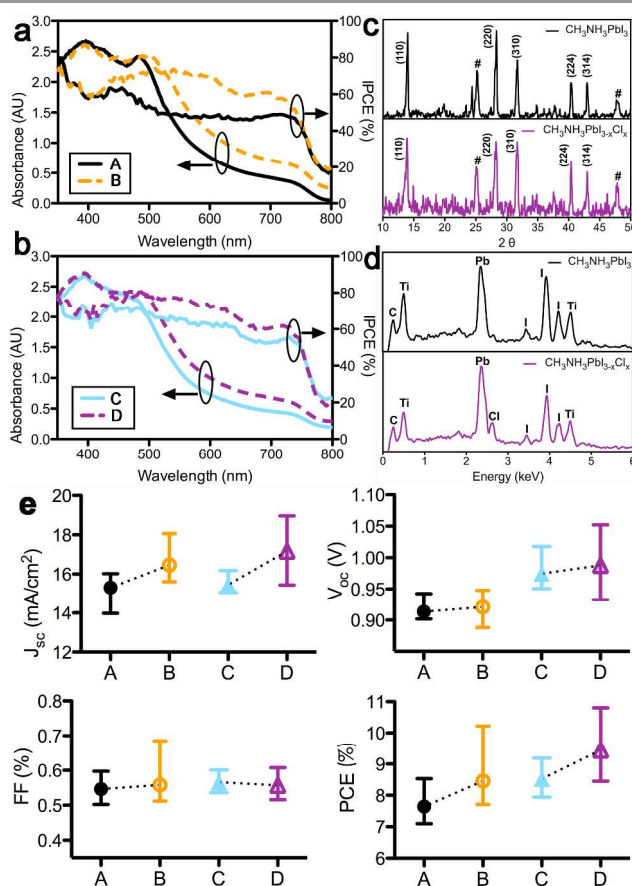


Figure 3. a) The absorption spectra and IPCE of a) $\text{CH}_3\text{NH}_3\text{PbI}_3$ and b) $\text{CH}_3\text{NH}_3\text{PbI}_{3-x}\text{Cl}_x$ device. c) XRD spectra and d) EDS spectra of the perovskite films on top of the mesoporous TiO_2 , hashes indicate the peaks ascribed to TiO_2 . e) The photovoltaic performances of Device A-D. Each data point represents the average of a set of at least 20 individual devices.

The absorption spectra showed Film B has stronger light harvesting from 490 nm to 800 nm than Film A (Figure 3a), while in 350-490nm, they have comparable absorptive intensity. This indicates the same perovskite quantity in two films, thus the additional absorption all results from the efficient light scattering effect of the rough surface. The effective optical path length of device has increased by the textured surface of large perovskite crystallites.⁵ Moreover, the charge transporting property can also be improved in Film B. Firstly, the continuous crystallites with larger size enhanced the degree of ordering inside the film,³⁰ so that the excellent transporting properties of perovskite materials could be better utilized. Secondly, the interpenetration of perovskite and spiro-MeOTAD provided richer interfaces for excitons to separate. These conclusions are correspondence with the results of incident photon to current conversion efficiency (IPCE), which not only increased in 490-800 nm, but also in the area of < 490 nm without enhancement of light absorption.

In order to compare the device performances more objectively, at least 20 individual devices both with and without the rough interface were fabricated and measured under AM 1.5G sun illumination (100 mW cm⁻²). Figure 3e shows the average device performance and the error bars based on the structure: FTO/compact TiO₂/mesoporous TiO₂/CH₃NH₃PbI₃/spiro-MeOTAD/Ag. Benefiting from the rougher interface of perovskite/HTM, the average J_{sc} increased from 15.3 mA cm⁻² (Device A) to 16.5 mA cm⁻² (Device B), with almost unchanged V_{oc} and FF . The average PCE increased from 7.6% to 8.4% as well.

To exclude the effect brought by different crystal type of perovskite, XRD data was measured to prove the perovskite in the same tetragonal ($I4/mcm$) symmetry at both 25 °C and 50 °C (Figure 3c).³⁰⁻³² According to T. Baikie's research, the tetragonal perovskite becomes cubic at the temperatures of 54-57 °C. That's why no higher than 50 °C have been considered as the high reaction temperature.³⁰

Table 1. The photovoltaic performances^a of Device A-G.

Device	V_{oc} (V)	J_{sc} (mA cm ⁻²)	FF	PCE (%)
A	0.91	15.3	0.55	7.6
B	0.92	16.5	0.56	8.4
C	0.97	15.5	0.57	8.5
D	0.99	17.2	0.56	9.5
E	0.93	14.8	0.45	6.2
F	0.88	17.5	0.48	7.4
G	0.74	15.8	0.49	5.7

^aThe average of a set of at least 20 individual devices. The performances of each device are listed in Table S1†

The conditions to form the rougher interface are also suitable for the Cl-doped hybrid perovskite of CH₃NH₃PbI_{3-x}Cl_x ($x \approx 0.5$), approximately deduced from the energy dispersive spectra (EDS) as shown in Figure 3d) by sequential deposition. By reacting films of PbI₂/PbCl₂ mixtures with CH₃NH₃I at 25 °C (Film C) and 50 °C (Film D), rougher surface of the perovskite layers have been obtained in Film D, with the similar SEM image to Film B (Figure S1†). Obvious higher absorption

spectra and IPCE are observed for Device D (from Film D) than Device C (from Film C) over the range of 470-750 nm (Figure 3b). The maximum IPCE of Device D at 500 nm is over 80%. The average J_{sc} of Device D reached 17.2 mA cm⁻², 1.7 mA cm⁻² higher than that of Device C, with the average PCE increasing from 8.5% to 9.5%. XRD data confirmed no change on crystal type if perovskite crystallites were forming at 50 °C. Compared to CH₃NH₃PbI₃ devices, the average J_{sc} of CH₃NH₃PbI_{3-x}Cl_x devices are unanimous larger (Figure 3e), probably due to the longer charge diffusion length and improved charge transport properties of CH₃NH₃PbI_{3-x}Cl_x.^{9,32}

Since the control condition to make the rough surface is only about the process of crystal formation, it is also applicable to devices without the mesoporous structure. The devices based on structure: FTO/compact TiO₂/CH₃NH₃PbI₃/spiro-MeOTAD/Ag were also fabricated by forming CH₃NH₃PbI₃ at 25 °C and 50 °C. Rough interface and enhancement of J_{sc} and PCE can be obviously observed for devices under the reaction at 50 °C (Figure S2†). These results indicate that to introduce a rough interface of perovskite/HTM is a universal way to increase the short-circuit current and PCE of perovskite solar cells without the necessary of mesostructure.

2. Pre-wetting time control

From the previous conclusions, the rough interfaces of perovskite/HTM is advantageous to the J_{sc} . Meanwhile, controlling the pre-wetting time can also be used to adjust the roughness of surface.²⁹ By changing the pre-wetting time from 0s (Film E), 2 s (Film A) to 5 s (Film F) and 10 s (Film G), the perovskite crystallites grew from 100nm of in-plane grain size for Film E to about 200nm for Film A, 350 nm for Film F and 1 μm for Film G (Figure 4), and turned into rough surfaces in Film F and G. Accordingly, the 3D topographic images (Figure S3b†) displayed gradual increases of roughness with prolonging the pre-wetting time. The calculated rms roughness for Film E, A, F, G, were 44.1 nm, 44.5 nm, 87.8 nm, 118 nm, respectively (Figure S3c†). However, the enlargement of perovskite crystallites was accompanied with loose arrangement of the crystallites and the bareness of the mesoporous TiO₂, which was different from the changes taken by temperature.

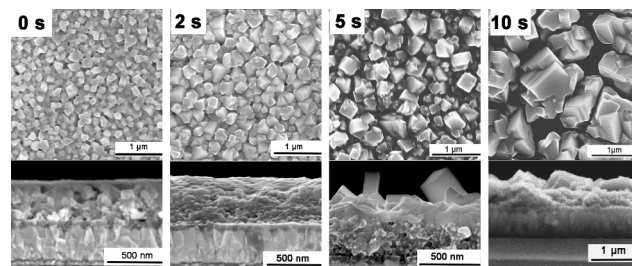


Figure 4. Top-view and cross-sectional SEM images of the perovskite layer on top of the mesoporous TiO₂ by different pre-wetting time of 0 s, 2 s, 5 s, 10 s corresponding to Film E, A, F, G.

According to the absorption spectra, Film F and G showed additional absorption than Film A and E, especially Film G, with strong light scattering from the 500 nm to 800nm (Figure

5a). As a consequence, Device F (from Film F) and Device G (from Film G) displayed distinctly higher J_{sc} than Device A (from Film A), and Device E (from Film E) without pre-wetting showed the poorest J_{sc} . Device F gave the highest average J_{sc} of 17.5 mA cm^{-2} , even 1.7 mA cm^{-2} higher than Device G, although its absorbance was weaker than that of Film G (Figure 5b). This can be explained by the SEM image of Film G. As the isolated crystallites are with size of $1 \mu\text{m}$, far more than 100 nm of the charge diffusion length of $\text{CH}_3\text{NH}_3\text{PbI}_3$,^{9,10} the electron and hole recombination becomes more serious. Crystallites in Device B and F had the same size of 350 nm , and achieved the highest in each group, indicating that $\sim 350 \text{ nm}$ maybe a suitable size of perovskite crystallites for solar cells.¹⁹

However, Device A showed the highest average PCE of 7.6% with the lowest average J_{sc} of 15.3 mA/cm^2 . This mismatch derived from the V_{oc} loss caused by the partially direct contacting between the HTM and the bare mesoporous TiO_2 in Device F and G.^{11,33} Hence, high coverage of TiO_2 is crucial and essential to achieve high PCEs, and short pre-wetting time can make sure fully coverage of the TiO_2 .

Through the control of pre-wetting time, we also realized the rough interface of perovskite/HTM and the enhancement of J_{sc} by the light scattering. But the continuity of the perovskite film has been destroyed and the TiO_2 was bared, which led to a seriously unfavorable impact on the V_{oc} and PCE. The research of pre-wetting step reminds us an important factor cannot be ignored in fabricating the device with a rough interface.

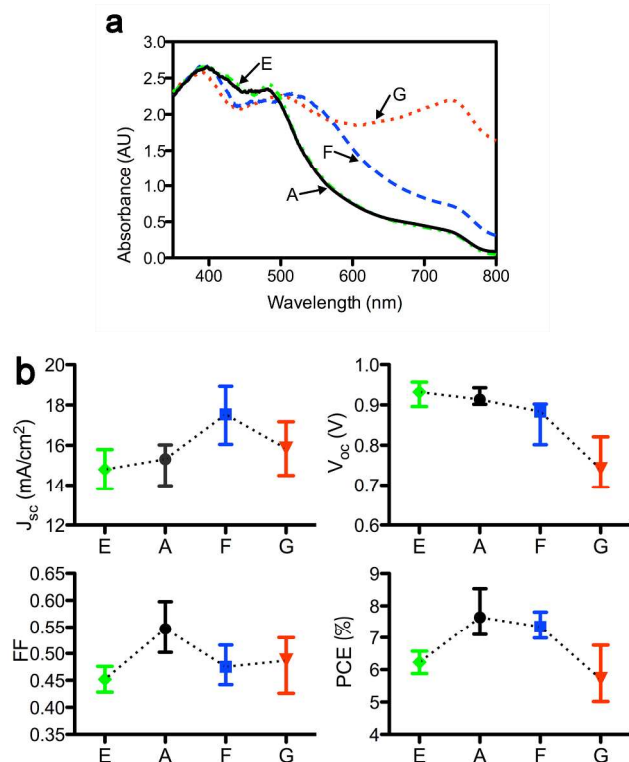


Figure 5. a) The absorption spectra of Film E, A, F, G. b) The photovoltaic performances of Device E, A, F, G. Each data point represents the average of a set of 20 individual devices.

As the discussion all above, reaction temperature mainly affects the size of perovskite crystallites, while pre-wetting time affects both size and compact degree of crystallites. A rough but also continuous interface of perovskite/HTM can be fabricated by increased reaction temperature and shortened pre-wetting time. Benefiting from improved light absorption and charge transport, the best performances of optimized devices containing a rough interface reached PCEs of 10.2% and 10.8% for $\text{CH}_3\text{NH}_3\text{PbI}_3$ and $\text{CH}_3\text{NH}_3\text{PbI}_{3-x}\text{Cl}_x$, respectively (Figure 6).

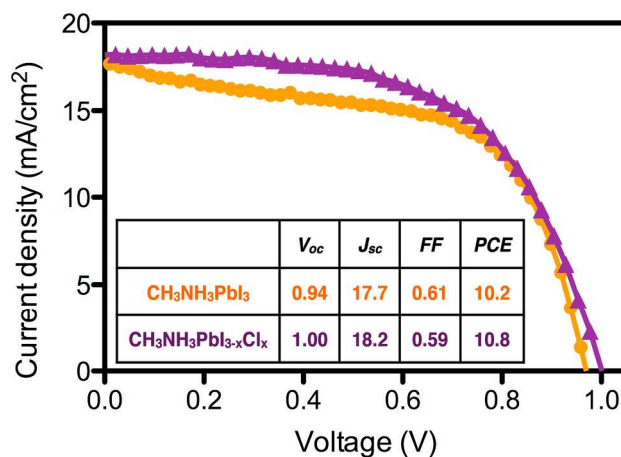


Figure 6. The best photovoltaic performances of the devices with a rough interface of perovskite/HTM.

Conclusions

In summary, we successfully fabricated the perovskite solar cell containing a rough interface of perovskite/HTM. Pre-wetting time and reaction temperature were systematically investigated to control the morphology of the perovskite film on TiO_2 . The expected solar cells with a rough as well as continuous interface of perovskite/HTM were obtained at the higher reaction temperature of $50 \text{ }^\circ\text{C}$, with the pre-wetting time of 2 s . Due to the improved light harvesting and charge transporting properties, the J_{sc} and PCE increased simultaneously without changing the thickness and the complexity of the device. Accordingly, the best performing devices have been achieved with PCE of 10.2% and 10.8% for $\text{CH}_3\text{NH}_3\text{PbI}_3$ and $\text{CH}_3\text{NH}_3\text{PbI}_{3-x}\text{Cl}_x$, respectively. This work suggests an effective way for perovskite solar cells to make full use of incident light and improve the charge transporting property. The results have been proved to be consistent for both $\text{CH}_3\text{NH}_3\text{PbI}_3$ and $\text{CH}_3\text{NH}_3\text{PbI}_{3-x}\text{Cl}_x$ based solar cells, and it is also appropriate for perovskite solar cells by sequential deposition with various structures.

Experimental details

$\text{CH}_3\text{NH}_3\text{I}$ Preparation. Based on the literature¹⁸, hydroiodic acid (114 mmol , 15 mL , $57 \text{ wt}\%$) and methylamine (140 mmol , 70 mL , 2 M in methanol) were reacted at $0 \text{ }^\circ\text{C}$ with stirring under N_2 for 120 min . The resultant solution was evaporated to give a white precipitate, then washed with diethyl ether and

dried under vacuum and used for the following step without further purification.

Device Fabrication. Fluorine doped tin oxide (FTO) glass was cleaned as previously reported³⁴ via sequentially in detergent, water, acetone, and ethanol under ultrasonication for 15 min, and then treated with O₂ plasma for 15 min. The following procedure was modified on the base of literature.⁴ A compact TiO₂ layer on the FTO glass was prepared by spin-coating of titanium diisopropoxide bis(acetylacetonate) solution (0.15 M, in 1-butanol) at 4,000 r.p.m. for 30 s, dried at 125 °C for 5 min, then repeated twice with 0.3 M of titanium diisopropoxide bis(acetylacetonate) solution, finally baked at 500 °C for 15 min. After then, the resultant TiO₂ film was immersed into a 40 mM TiCl₄ aqueous solution at 70 °C for 30 min, washed with deionized water and ethanol, then baked at 500 °C for 15 min. The mesoporous TiO₂ film was prepared by spin-coating a 20-nm-sized TiO₂ paste (diluted in ethanol with a ratio of 2:7 by weight, Heptachroma, DHS-TPP3) at 4,000 r.p.m. for 30 s, dried at 125 °C for 5 min, then heated at 500 °C for 15 min. The mesoporous TiO₂ films were filled by spin-coating of 1M PbI₂ solution (Film A, B, E, F, G) in DMF at 3000 r.p.m. or 1M PbI₂/PbCl₂ (1:1) mixed solution (Film C, D) in DMF at 2500 r.p.m. that was kept at 70 °C. After drying at 70 °C, the films were pre-wetted by 2-propanol for 0 s (Film E), 2 s (Film A, B, C, D), or 5 s (Film F), or 10 s (Film G), before dipped into 10mg/mL CH₃NH₃I solution kept at R.T. (Film A, C, E, F, G) or 50 °C (Film B, D) for tens of seconds. A solution of 2,2',7,7'-tetrakis(*N,N*-di-*p*-methoxyphenylamine)-9,9'-spirobifluorene (spiro-MeOTAD), 4-*tert*-butylpyridine (96%, Aldrich), and lithium bis(trifluoromethylsulphonyl)imide (98%, Alfa Aesar) in chlorobenzene (99.9%, Alfa Aesar) was spin-coated at 2000 r.p.m. for 60 s as the HTM. Finally, 80 nm Ag was thermally evaporated under vacuum to act as the cathode.

Measurements. The absorption spectrum was recorded with UV-visible spectrophotometer (Agilent 8453). The morphology was measured by scanning electron microscope (SEM) (FEI Nova_NanoSEM430 and HITACHI 4300) and atomic force microscopy (AFM) (Agilent Series 5500). The EDS spectra were performed on Nova_NanoSEM430. The XRD spectra were obtained from a Philips X'PERT-MRD x-ray diffractometer. Photovoltaic performances were measured by using Keithley 2611 source meter under simulated sunlight from Oriol 300 solar simulator. IPCE was measured by using a lock-in amplifier coupled with a monochromator and 500 W xenon lamp (Crowntech, Qtest Station 2000). Both two systems were calibrated against a certified reference solar cell. All the measurements of the solar cells were performed under ambient atmosphere at room temperature without encapsulation.

Acknowledgements

This study was partly financially supported by the National Natural Science Foundation of China (10934001, 61177020, 11074016, 11121091, 61275034 and 61106123) and the

National Basic Research Program of China (2013CB328700). The authors are thankful to Mr. Xiao Yu and Prof. Dechun Zou in the College of Chemistry and Molecular Engineering of Peking University for their kindly help in the assistance in the measurements of SEM images.

Notes and references

^a State Key Laboratory for Mesoscopic Physics and Department of Physics, Peking University, Beijing 100871, China

^b New Display Device and System Integration Collaborative Innovation Center of the West Coast of the Taiwan Strait, Fuzhou 350002, China

^c Key Laboratory of Photonics Technology for Information, Key Laboratory for Physical Electronics and Devices of the Ministry of Education, Department of Electronic Science and technology, School of Electronic and Information Engineering, Xi'an Jiaotong University, Xi'an, 710049, China

† Electronic Supplementary Information (ESI) available: SEM images of CH₃NH₃I_{3-x}Cl_x by different reaction temperature; SEM images of perovskite on compact TiO₂ by different reaction temperature; AFM 3D topographic images and calculated roughness; Stability of devices; all performance of each device. See DOI: 10.1039/b000000x/

- 1 A. Kojima, K. Teshima, Y. Shirai and T. Miyasaka, *J. Am. Chem. Soc.*, 2009, **131**, 6050-6051.
- 2 M. M. Lee, J. Teuscher, T. Miyasaka, T. N. Murakami and H. J. Snaith, *Science*, 2012, **338**, 643-647.
- 3 H. S. Kim, C. R. Lee, J. H. Im, K. B. Lee, T. Moehl, A. Marchioro, S. J. Moon, R. Humphry-Baker, J. H. Yum, J. E. Moser, M. Grätzel and N. G. Park, *Sci. Rep.*, 2012, **2**, 591.
- 4 J. Burschka, N. Pellet, S.-J. Moon, R. Humphry-Baker, P. Gao, M. K. Nazeeruddin and M. Grätzel, *Nature*, 2013, **499**, 316-319.
- 5 D. Liu and T. L. Kelly, *Nature Photonics*, 2014, **8**, 133-138.
- 6 H. J. Snaith, *J. Phys. Chem. Lett.*, 2013, **4**, 3623-3630.
- 7 W. Zhang, M. Saliba, S. D. Stranks, Y. Sun, X. Shi, U. Wiesner and H. J. Snaith, *Nano Lett.*, 2013, **13**, 4505-4510.
- 8 P. Qin, A. L. Domanski, A. K. Chandiran, R. Berger, H.-J. Butt, M. I. Dar, T. Moehl, N. Tetreault, P. Gao, S. Ahmad, M. K. Nazeeruddin and M. Grätzel, *Nanoscale*, 2014, **6**, 1508.
- 9 S. D. Stranks, G. E. Eperon, G. Grancini, C. Menelaou, M. J. P. Alcocer, T. Leijtens, L. M. Herz, A. Petrozza and H. J. Snaith, *Science*, 2013, **342**, 341-344.
- 10 G. Xing, N. Mathews, S. Sun, S. S. Lim, Y. M. Lam, M. Grätzel, S. Mhaisalkar and T. C. Sum, *Science*, 2013, **342**, 344-347.
- 11 G. E. Eperon, V. M. Burlakov, P. Docampo, A. Goriely and H. J. Snaith, *Adv. Funct. Mater.*, 2014, **24**, 151-157.
- 12 T. Leijtens, G. E. Eperon, S. Pathak, A. Abate, M. M. Lee and H. J. Snaith, *Nature Communications*, 2013, DOI: 10.1038/ncomms3885.
- 13 K. Wojciechowski, M. Saliba, T. Leijtens, A. Abate and H. J. Snaith, *Energy Environ. Sci.*, 2014, **7**, 1142.
- 14 J. H. Noh, S. H. Im, J. H. Heo, T. N. Mandal and S. I. Seok, *Nano Lett.*, 2013, **13**, 1764-1769.
- 15 H.-S. Kim, J.-W. Lee, N. Yantara, P. P. Boix, S. A. Kulkarni, S. Mhaisalkar, M. Grätzel and N.-G. Park, *Nano Lett.*, 2013, **13**, 2412-2417.
- 16 M. Liu, M. B. Johnston and H. J. Snaith, *Nature*, 2013, **501**, 395-398.

- 17 A. Abrusci, S. D. Stranks, P. Docampo, H.-L. Yip, A. K. Y. Jen and H. J. Snaith, *Nano Lett.*, 2013, **13**, 3124–3128.
- 18 J. H. Heo, S. H. Im, J. H. Noh, T. N. Mandal, C.-S. Lim, J. A. Chang, Y. H. Lee, H.-j. Kim, A. Sarkar, M. K. Nazeeruddin, M. Grätzel and S. I. Seok, *Nat. Photonics*, 2013, **7**, 486–491.
- 19 Q. Chen, H. Zhou, Z. Hong, S. Luo, H.-S. Duan, H.-H. Wang, Y. Liu, G. Li and Y. Yang, *J. Am. Chem. Soc.*, 2013, **136**, 622–625.
- 20 O. Malinkiewicz, A. Yella, Y. H. Lee, G. M. Espallargas, M. Grätzel, M. K. Nazeeruddin and H. J. Bolink, *Nat. Photonics*, 2013, **8**, 128–132.
- 21 C. Wehrenfennig, G. E. Eperon, M. B. Johnston, H. J. Snaith and L. M. Herz, *Adv. Mater.*, 2013, DOI: 10.1002/adma.201305172.
- 22 P. Docampo, J. M. Ball, M. Darwich, G. E. Eperon and H. J. Snaith, *Nature Communications*, 2013, **4**, 2761.
- 23 B. Conings, L. Baeten, C. D. Dobbelaere, J. D’Haen, J. Manca and H.-G. Boyen, *Adv. Mater.*, 2013, DOI: 10.1002/adma.201304803.
- 24 G. Li, V. Shrotriya, J. Huang, Y. Yao, T. Moriarty, K. Emery and Y. Yang, *Nature Materials*, 2005, **4**, 864–868.
- 25 M. Graetzel, R. A. J. Janssen, D. B. Mitzi and E. H. Sargent, *Nature*, 2012, **488**, 304–312.
- 26 J. Müller, B. Rech, J. Springer and M. Vanecek, *Solar Energy*, 2004, **77**, 917–930.
- 27 K. Zhu, N. R. Neale, A. Miedaner and A. J. Frank, *Nano Lett.*, 2007, **7**, 70–74.
- 28 P. Qiang, P. Yang, Z. Liang, Y. Luo, J. Yu, Y. Lan, X. Cai, S. Tan, P. Liu and W. Mai, *Journal of Alloys and Compounds*, 2014, **583**, 300–304.
- 29 G. Dhanaraj, K. Byrappa, V. Prasad and M. Dudley, in *Springer Handbook of Crystal Growth*, Eds. F. Abbona and D. Aquilano, Springer, Berlin Heidelberg, 2010, pp 53–87.
- 30 T. Baikie, Y. Fang, J. M. Kadro, M. Schreyer, F. Wei, S. G. Mhaisalkar, M. Grätzel and T. J. White, *J. Mater. Chem. A*, 2013, **1**, 5628–5641.
- 31 C. C. Stoumpos, C. D. Malliakas and M. G. Kanatzidis, *Inorg. Chem.*, 2013, **52**, 9019–9038.
- 32 S. Colella, E. Mosconi, P. Fedeli, A. Listorti, F. Gazza, F. Orlandi, P. Ferro, T. Besagni, A. Rizzo, G. Calestani, G. Gigli, F. D. Angelis and R. Mosca, *Chem. Mater.*, 2013, **25**, 4613–4618.
- 33 H. J. Snaith, N. C. Greenham and R. H. Friend, *Adv. Mater.*, 2004, **16**, 1641–1645.
- 34 L. Zhang, X. Xing, Z. Chen, L. Xiao, B. Qu and Q. Gong, *Energy Technol.* 2013, **1**, 613–616.